ICIC Express Letters
Part B: Applications
Volume **7**, Number **1**, January **2016**

ICIC International ©2016 ISSN 2185-2766
pp. **159–166**

A MULTI-FRACTAL MULTI-PERMUTED MULTINOMIAL MEASUREMENT FOR UNSUPERVISED IMAGE SEGMENTATION

Sung-Tsun Shih and Lui Kam

Department of Electronic Engineering
Cheng-Shiu University
No. 840, Cheng-Chin Rd., Niaosong Dist., Kaohsiung 83347, Taiwan
stshih@gcloud.csu.edu.tw

Received June 2015; accepted August 2015

Abstract. *By extending multinomial measures, a new class of self-similar multi-fractal measures is developed for texture representation. Two multi-fractal features have been shown to be suitable for texture discrimination and classification. Their use within a supervised segmentation framework provides us with satisfactory results. In this paper, we complete the survey on these features by showing their rotation invariant property and their scaling behavior. Both properties are particularly important for analyzing aerial images because the geographical elements can appear in different orientations and scales. Then, an automatic clustering algorithm based on a watershed technique is used for the segmentation of real world images. The experimental results are encouraging. Through this study, the multi-fractal measures we developed demonstrate a relevant characterization of natural textures by only two attributes. They are rotation invariant and possess a good behavior with respect to the scaling ratio. These properties reinforce the reliability of these two attributes for aerial or satellite image characterization.*
Keywords: Multi-fractal, Multinomial measurement, Unsupervised image segmentation

1. **Introduction.** Analyzing and interpreting images by means of texture attributes is a widespread method including many approaches like statistical characterization [8,10], filtering techniques [3,15], geometric models [20,22], fractal geometry [2,13,21], or multi-fractal analysis [16,19,23]. Each of them is well adapted only to a specific application.

In previous work [11], the use of cooccurrence statistics [10] is shown to give poor segmentation results on aerial images. A straightforward application of fractal features (fractal dimension, lacunarity) proves them inappropriate for this purpose. Nevertheless, each geographical element exhibits a kind of statistical self-similarity in its own way. Several works [14,18] suggested computing local fractal dimension for the improvement of the segmentation results. Hence, the multi-fractal analysis, which is a generalization of the fractal geometry, is well adapted to the description of the aerial and satellite images.

The former works of Lévy-Véhel et al. [16,17] introduced a multi-fractal approach for image segmentation. The analysis of an image is based on local Hölder exponents (with respect to a measure or a Choquet capacity) and the multi-fractal spectrum (global information). Although these mathematical tools can provide relevant information for image analysis, we must emphasize on the fact that we do not know which measure or capacity to choose in practice. Furthermore, the computation of the local Hölder exponents and the multi-fractal spectrum must rely on estimators and is time consuming in most of cases.

A multi-fractal measure is developed in [11] for segmenting real world images. The theoretical background and some useful properties of this model are reviewed briefly in the next section, and an estimator for the inverse problem of parameters identification is defined. The use of this estimator on several natural textures provides us with meaningful results. In Section 3, we first recall the main results related to the texture characterization

by using two multi-fractal features. As the aerial scenes are shaped by man-made objects (urban areas, open countries) and natural elements (water-courses, vegetation) which can occur at different scales and orientations, this survey is completed by studying the scaling behavior and the rotation invariance of both texture descriptors. Then, after a short review of the classical methods of data clustering, we describe the unsupervised algorithm we proposed for the segmentation of images. Experimental results are given in Section 4.3. The limits of our model and future investigations are detailed as a conclusion.

2. **Multi-fractal Texture Model.** The multinomial measures are well studied self-similar measures [7]. They can be generated as the limit of multiplicative cascaded processes. By introducing spatial per-mutations into each stage of the underlying processes, we extended the multinomial measures to so called *Multi-permuted Multinomial Measures* (or MMM).

2.1. **Definitions and properties.** More formally, let $N_p(n)$ be the set of the first p^n non negative integers and $C_0 = [0,1)^2$ be the support of the measure. Given p^2 masses $P_{i,j}$ $(i,j \in N_p(1))$, whose total sum is 1, the pyramidal construction of an MMM (denoted by $\mu\Pi_p$) is based on an iterative splitting of C_0 associated with a multiplicative rule between successive stages.

At the first stage, $C_0 = [0,1)^2$ (with measure 1) is partitioned regularly into p^2 subsets C^1_{ij} whose measure is $P_{i,j}$. The same splitting procedure is carried out on these subsets at the next stage, yielding $\left(p^2\right)^2$ new subsets $C^2_{k_i,l_j}$ with a measure defined by a multiplicative rule:

$$\forall n \geq 1,\ \mu\Pi_p\left(C^{n+1}_{k_i,l_j}\right) = P_{\pi^n_{i,j}(k,l)}\mu\Pi_p\left(C^n_{i,j}\right) \tag{1}$$

with $k_i = \lfloor (i+1)/p \rfloor + k$ and $l_j = \lfloor (j+1)/p \rfloor + l$ ($\lfloor x \rfloor$ is the integer part of x). $\pi^n_{i,j}$ is a permutation related to $C^n_{i,j}$ at the stage n, acting on the position of the masses $P_{i,j}$ for the multiplicative rule involved at the stage $n+1$. By iterating this process ad infinitum, one gets an MMM.

Figure 1 displays the first 2 steps of the cascaded process of an MMM with $p = 3$ and $\pi^1_{1,1}(k,l) = (l,k)$. One can notice that the limit measure is a multinomial measure iff all the permutations are equal to the identity function.

Its multifractality can be determined through a repartition function [9] defined at stage n as:

$$\Gamma_n(q,\tau) = \sum_{i,j \in N_p(n)} \frac{\left[\mu\Pi_p\left(C^n_{i,j}\right)\right]^q}{p^{-2n\tau}} \tag{2}$$

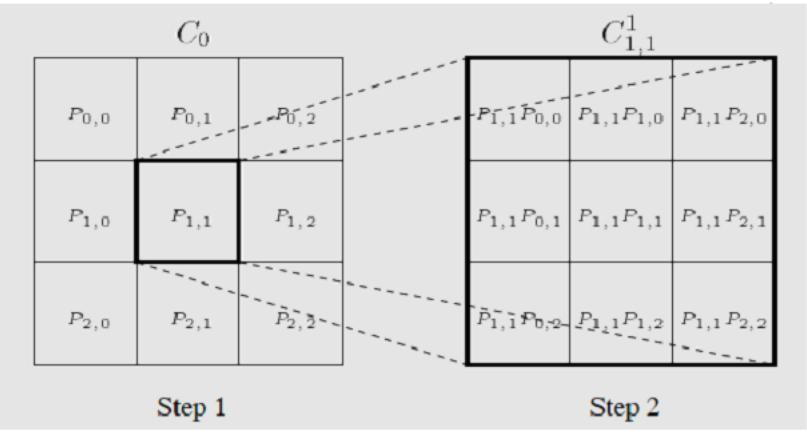

FIGURE 1. Steps 1 and 2 of an MMM's cascade

There exists a unique function $\tau(q)$, called Rényi exponent, such that $\Gamma_n(q, \tau(q)) = 1$. It characterizes the multi-fractal behavior of a singular measure. Since the permutations operate only on the position of the masses $P_{i,j}$ at each stage, the set of measures $\mu\Pi_p(C_{i,j}^n)$ remains invariant.

Thus, the Rényi exponent of an MMM and its corresponding multinomial measure are identical. Moreover, the MMMs are self-similar (modulo permutations) by construction. The set of the local Hölder exponents and the multi-fractal spectrum are simply related to the Rényi exponent by the Legendre transform (see [7]). This remark is very important for the computation of the multi-fractal features because they can be determined analytically once the parameters of the model are identified.

2.2. **Inverse problem.** An MMM is completely defined by the knowledge of the integer p, the p^2 masses $P_{i,j}$ and the permutations. A fast algorithm is developed in [11] for the masses estimation:

$$\widetilde{P}_{i,j} = \frac{1}{1 + N_\pi(p, n_0)} \sum_{n=0}^{n_0-1} \sum \widetilde{P}_{\pi_{i,j}^n(k,l)} \tag{3}$$

The values $\widetilde{P}_{\pi_{i,j}^n(k,l)}$ correspond to the estimates of the permuted masses observed at iteration n. They can be computed according to Equation (1). $N_\pi(p, n_0)$ is the number of permutations achieved after n_0 iterations:

$$N_\pi(p, n_0) = \sum_{n=2}^{n_0} \left(p^2\right)^{n-1} = \frac{p^{2n_0} - p^2}{p^2 - 1} \tag{4}$$

The permutations can be determined at the same time as the estimation of the permuted masses. Indeed, the sorting of the estimates $\widetilde{P}_{\pi_{i,j}^n(k,l)}$ yields a mapping between the initial and the permuted positions of the masses.

The method described above is applicable if p and n_0 are known *a priori*. Their choice depends both on the intrinsic characteristics of the images and on the application considered. In order to avoid texture mixing within an analyzing window, we suggested taking small values of p and n_0 (respectively 3 and 2) for an accurate segmentation [11].

2.3. **Approximating textures.** Our first goal was to find a relevant multi-fractal representation for texture characterization. In order to evaluate the relevance of the MMM model for texture approximation, several natural textures – drawn from the Brodatz album and the image database of SIPI (Signal and Image Processing Institute) of the USC – are used as testing images. Figure 2 shows a sample of 4 original textured images (grass,

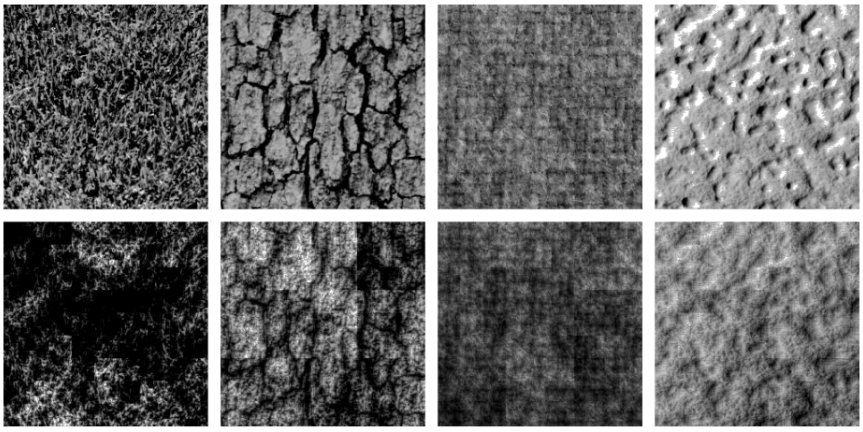

FIGURE 2. Four natural textures (D9, D12, D19, T3) and their approximations by $\mu\Pi_3$

bark, wool and rough wall) and their corresponding approximation computed by $\mu\Pi_3$ with $n_0 = 5$ iterations.

Some artifacts (square blocks) can be observed on the synthesized images. They are due to the regular iterated splitting of C_0. However, as well as micro-textures (grass, wool) or macro-textures (bark, rough wall), the MMM approximations preserve quite correctly their geometric structures thanks to the effect of the permutations.

3. Texture Attributes.

The multi-fractal analysis of an MMM can also be achieved by means of the multi-fractal spectrum approach (see 2.1) which gives both local and global information.

3.1. Previous results.

This huge amount of information has been largely reduced as only 2 attributes are extracted, namely the extreme of the local Hölder exponents [7]:

$$\alpha_{\min} = -\log\left(\max_{i,j} P_{i,j}\right)/2\log p, \tag{5}$$

$$\alpha_{\max} = -\log\left(\min_{i,j} P_{i,j}\right)/2\log p. \tag{6}$$

They are directly related to the parameters of the model and should give a good characterization of the model.

In [11], these texture attributes are computed (with $p = 3$ and $n_0 = 5$) on 100 subimages (of size 243^2) extracted from each of the 13 Brodatz textures: grass, bark, straw, textile, wool, pressed calf leather, sand, water, wood, raffia, pigskin, wall bricks and bubbles. Here, we add 3 more textures (called T1, T2, T3) retrieved from the image database of the SIPI: hexagonal holes, gravels and rough wall.

The $(\alpha_{\min}, \alpha_{\max})$ plot of these textures is displayed in Figure 3. Most of the clusters are separated from the others, except those of the textures D19 and D84 (resp. D92 and T2). In fact, if one examines these pairs of textures, their patterns look similar. For instance, D19 and D84 are both structured micro-textures whose patterns are about the same size. As for D92 and T2, they are non-structured macro-texture also with equivalent pattern size.

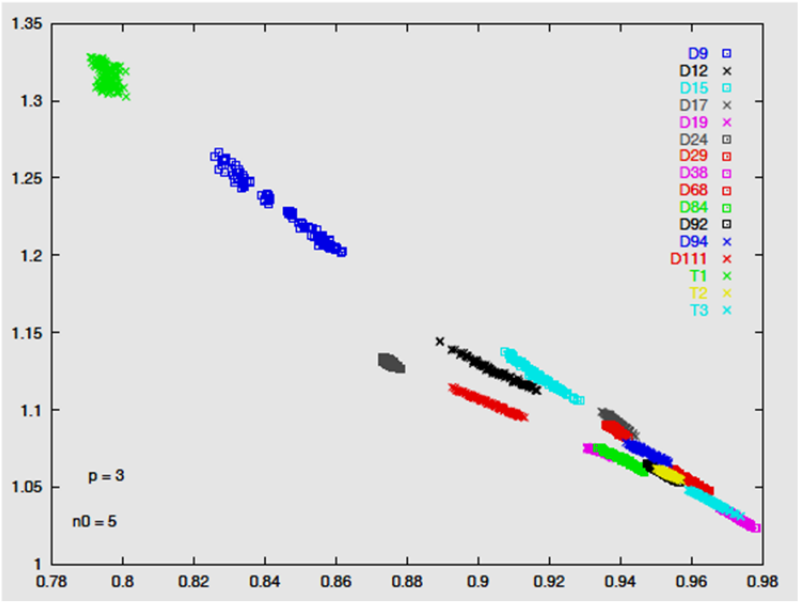

FIGURE 3. $(\alpha_{\min}, \alpha_{\max})$ plot computed for each of the 16 Brodatz and Brodatz-like textures

Furthermore, the spatial arrangement of the clusters is directly related to the visual irregularities of the textures. Indeed, the most irregular (D9) or contrasted (T1) textures have their clusters located on the top left corner of the $(\alpha_{\min}, \alpha_{\max})$ plot. Whereas the clusters of the smoother textures (D38) are located near the right bottom corner. This phenomenon can be explained by the fact that irregular or contrasted textures have a wide range of local irregularities (i.e., small $\alpha_{\min}$ and large $\alpha_{\max}$ values). The opposite behavior is observed for the smoother textures.

3.2. **Scaling behavior.** Our multi-fractal attributes should be scale invariant according to the theory. For each textured image, we studied this behavior over a set of 5 images of size 243^2, 365^2, 486^2, 608^2 and 729^2 zoomed in or out from the original 512^2 sized image by a bi-cubic interpolation. The ratio between the largest image and the smallest one is 3.

Again, $\alpha_{\min}$ and $\alpha_{\max}$ are computed from sub-images of size 243^2 for each zoomed image. The plots shown in Figure 4 reveal the representative (only 6 textures are considered for clarity) scaling behavior of the mean values of the attributes. When the scaling ratio increases, the 2 attributes are not as stable as predicted by the theory, but their variation does not exceed a few percent. Hence, we can assume that both attributes are relevant enough for texture characterization whatever the scale of observation is (in practice, a range of scales).

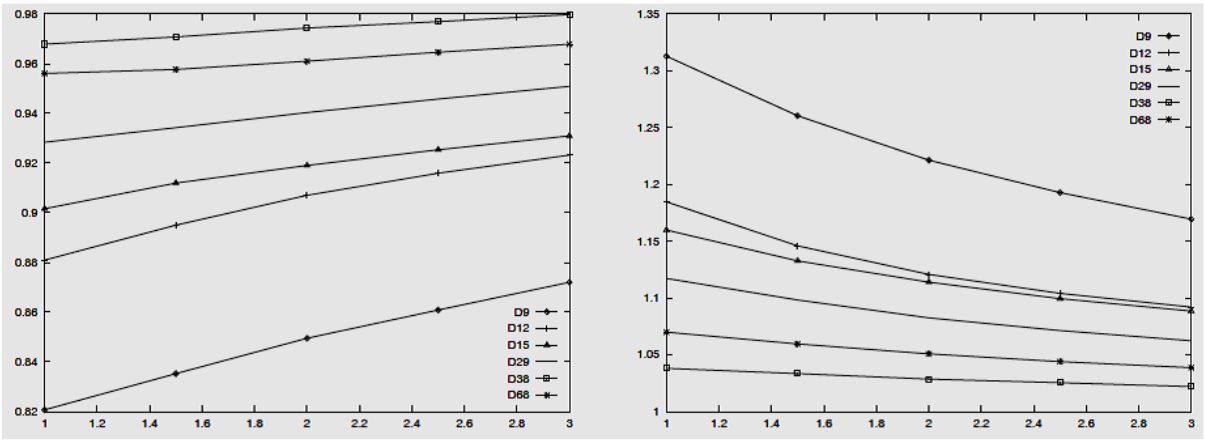

FIGURE 4. Scaling behavior of the mean values of $\alpha_{\min}$ (left) and $\alpha_{\max}$ (right) for 6 textures

3.3. **Rotation invariance.** The Hölder exponents characterize the local irregularities of a measure. If the support of the image is rotated, the irregularities should remain unchanged. This invariance property is investigated by testing images drawn from the SIPI image database in which the 13 Brodatz textures are scanned under 7 different angles: 0°, 30°, 60°, 90°, 120°, 150° and 200°. For the 3 other textures (T1, T2 and T3), the rotated images are generated by a bi-cubic interpolation.

The attributes are estimated for each rotated texture in the same manner as we do in the previous sections. Each cluster is modelled by a 2D Gaussian distribution whose means and covariance matrices are determined from the data. Whatever the rotated texture is, the coefficients of the covariance matrices are very small (10^{-4} to 10^{-6}): the clusters are compact and can be represented by the means.

For almost every texture (13 over 16), the variation of the 2 attributes with respect to the rotation angles does not exceed 10^{-2}. The less favorable case we can observe is that of the grass texture, but the variations are not excessive (maximum difference is about 006). According to these experimental results, we can conclude that $\alpha_{\min}$ and $\alpha_{\max}$ are stable enough under the rotation transformation.

4. **Unsupervised Segmentation.** The commonly used clustering techniques are based on K-means algorithm, hierarchical clustering, parametric or nonparametric density estimation [6]. After a short analysis of their advantages and shortcomings, we suggest a method based on the last approach for our segmentation problem.

4.1. **Clustering algorithms.** The K-means algorithm is a very fast and appropriate technique for large data sets. However, the number and the gravity centers of the effective clusters need to be specified correctly. If the clusters are unbalanced or elongated, small clusters may be absorbed by larger ones or conversely large clusters could be split into artificial sub-clusters.

Hierarchical clustering corresponds to an iterative merging which depends on the definition of a certain distance. At the beginning, the number of clusters is set equal to the number of data points. It decreases successively according to the merging criterion. For large data sets, the computation is very long.

By assuming that the underlying density of the data set results from a mixture of Gaussians, the parametric approach consists of estimating the means and the covariance matrices of these Gaussians. The effective number of clusters and the parameters of the Gaussians need to be initialized with accuracy. The commonly used methods are Expectation Maximization or Stochastic Expectation Maximization algorithms which spend lots of computation time.

4.2. **Nonparametric method.** This method is also based on the determination of the density of the data set without any analytical expression known. By convolving N data points $(X_1, \ldots, X_N)$ with a kernel function K [4,5], one gets the density function by:

$$f_N(x) = \frac{1}{Nh_N} \sum_{i=1}^{N} K\left(\frac{x - X_i}{h_N}\right) \tag{7}$$

h_N is the smoothing factor (width of K), its optimal choice depends on N and also on K [24]. The number of clusters is usually set to the number of local maxima of $f_N(x)$.

For our purpose, we chose the histogram calculation which is the simplest and the fastest nonparametric technique. The rectangular kernel K is centered on regularly spaced points X_i' (the data set is resampled) instead of X_i. Then, the reliability of the estimated density depends both on the resampling step and the smoothing factor h_N.

According to the definition of the MMM, $\alpha_{\min}$ and $\alpha_{\max}$ cannot take any values because the masses are constrained (total sum is 1). Thus, it is easier to fix *a priori* the resampling step and the smoothing factor. Assuming that the clusters corresponds to the principal modes of the histogram, a coarse resampling yields an approximation good enough and captures the low frequencies of the histogram.

Once the coarse density is determined, the data points are merged by a watershed technique [1,25] applied to the turned up histogram. The number of clusters is given by the number of basins. The watersheds define the cluster domains which lead to a segmentation of images.

4.3. **Experimental results.** We performed this unsupervised segmentation on satellite images and aerial photographs. For the histogram computation, the resampling step and the smoothing factor are respectively equal to 0.003 and 0.015.

As an example, the histogram related to the aerial photograph of Toride (middle image of Figure 5) is displayed in Figure 5. One can easily distinguish 4 visible modes but the algorithm gives us more clusters than expected (7 instead of 4) due to the boundary pixels. If we do not take them into account, the 4 modes observed on the histogram correspond to the effective clusters, namely the urban areas, the watercourses, the open countries and the vegetation.

FIGURE 5. (Left) Histogram of $(\alpha_{\min}, \alpha_{\max})$ related to the aerial photograph of Toride; (Middle and Right) Original and segmented aerial photograph of Toride

The right image of Figure 5 corresponds to the segmentation result. The 4 kinds of geographical elements are all rather well located. Of course, some pixels are misclassified (fields classified as watercourse), and this is due to the smoothness of those fields. In spite of this, the segmentation result is encouraging. All the more as the unsupervised segmentation algorithm found one more class (vegetation) than our supervised segmentation carried out in [11].

5. **Conclusions.** Through this study, the multi-fractal measures we developed demonstrate a relevant characterization of natural textures by only two attributes. They are rotation invariant and possess a good behavior with respect to the scaling ratio. These properties reinforce the reliability of these two attributes for aerial or satellite image characterization.

The 2 multi-fractal attributes are also used for segmenting simulated SPOT5 images and other non aerial textured images with outstanding results [12]. Of course, our method is ill-adapted if the local maxima of the histogram are too close or unbalanced. In that case, the coarse density estimation may not take into account the smaller ones which may lead to a poor segmentation result.

Although the 2 attributes are implicitly related to the permutations, we have to extend the study related to the effect of the permutations on the texture patterns. As the number of iterations is generally limited, a Markovian analysis cannot be considered. Thus, we shall define empirically a certain distance which is a very difficult task so as to reveal the geometric information carried by the permutations.

REFERENCES

[1] A. T. Alrawi, A Sagheer and D. A. Ibrahim, Texture segmentation based on multifractal dimension, *International Journal on Soft Computing*, vol.3, no.1, 2012.

[2] B. Chaudhuri and N. Sarkar, Texture segmentation using fractal dimension, *IEEE Trans. PAMI*, vol.17, no.1, pp.72-77, 1995.

[3] M. T. Alaoui and A. Sbihi, Fractal features classification for texture image using neural network and mathematical morphology, *Proc. of the World Congress on Engineering*, 2012.

[4] L. Devroye, *Nonparametric Density Estimation – The L1 View*, Wiley & Sons, New York, 1984.

[5] L. Devroye, The double kernel method in density estimation, *Annales de l'Institut Henri Poincar'e*, vol.25, pp.533-580, 1989.

[6] B. S. Everitt, *Cluster Analysis*, Edward Arnold, 1993.

[7] K. J. Falconer, *Techniques in Fractal Geometry*, Wiley & Sons, Chichester, 1997.

[8] A. Gagalowicz and C. Tournier-Lasserve, Third order model for non homogeneous natural textures, *IEEE ICIP*, pp.409-411, 1986.

[9] J. Hakansson and G. Russberg, Finite-size effects on the characterization of fractal sets: $f(\alpha)$ construction via box counting on a finite two-scaled Cantor set, *Physical Review A*, vol.41, no.4, pp.1855-1861, 1990.
[10] R. M. Haralick, K. Shanmugam and I. Dinstein, Textural features for image classification, *IEEE Trans. SMC*, vol.3, no.6, pp.610-621, 1973.
[11] L. Kam and J. Blanc-Talon, Multifractal texture characterization for real world image segmentation, *Advanced Concepts for Intelligent Vision Systems*, pp.45-50, 1999.
[12] L. Kam and J. Blanc-Talon, Multifractal texture segmentation for off-road robot vision, *Intelligent Systems: Theory and Applications*, IOS Press, Netherlands, 2000.
[13] J. M. Keller, S. Chen and R. M. Crownover, Texture description and segmentation through fractal geometry, *CVGIP*, vol.45, pp.150-166, 1989.
[14] J. M. Keller and Y. B. Seo, Local fractal geometric features for image segmentation, *International Journal of Imaging Systems and Technology*, vol.2, pp.267-284, 1990.
[15] K. I. Laws, Rapid texture identification, *SPIE Conference on Image Processing for Missile Guidance*, pp.376-380, 1980.
[16] J. Lévy-Véhel and P. Mignot, Multifractal segmentation of images, *Fractals*, vol.2, no.3, pp.371-377, 1994.
[17] J. Lévy-Véhel, P. Mignot and J. P. Berroir, Texture and multifractals: New tools for image analysis, *INRIA*, France, 1992.
[18] J. Maeda, V. V. Anh, T. Ishizaka and Y. Suzuki, Integration of local fractal dimension and boundary edge in segmenting natural images, *IEEE ICIP*, pp.845-848, 1996.
[19] P. Martinez, D. Schertzer and K. Pham, Texture analysis by universal multifractal features in a polarimetric SAR image, *IGARSS'96*, vol.1, pp.27-31, 1996.
[20] F. G. Peet and T. S. Sahota, Surface curvature as a measure of image texture, *IEEE Trans. PAMI*, vol.7, no.6, pp.734-738, 1985.
[21] A. P. Pentland, Fractal-based description of natural scenes, *IEEE Trans. PAMI*, vol.6, no.6, pp.661-674, 1984.
[22] S. Philipp and M. Smadja, Approximation of granular textures by quadric surfaces, *Pattern Recognition*, vol.27, no.8, pp.1051-1063, 1994.
[23] N. Sarkar and B. Chaudhuri, Multifractal and generalized dimensions of gray-tone digital images, *Signal Processing*, vol.42, pp.181-190, 1995.
[24] D. W. Scott, *Multivariate Density Estimation: Theory, Practice, and Visualization*, Wiley & Sons, New York, 1992.
[25] J. Serra, *Image Analysis and Mathematical Morphology*, Academic Press, London, 1982.